EARTHQUAKE ENGINEERING AND STRUCTURAL DYNAMICS
Earthquake Engng Struct. Dyn. 2005; **00**:1–20 *Prepared using* eqeauth.cls *[Version: 2002/11/11 v1.00]*

Direct Estimation of the Seismic Demand and Capacity of Oscillators with Multi-Linear Static Pushovers through IDA‡

Dimitrios Vamvatsikos[1,*,†] and C. Allin Cornell[2]

[1] *Department of Civil and Environmental Engineering, Univerisity of Cyprus, Nicosia 1678, Cyprus*
[2] *Department of Civil and Environmental Engineering, Stanford University, CA 94305-4020, U.S.A.*

SUMMARY

SPO2IDA is introduced, a software tool that is capable of recreating the seismic behavior of oscillators with complex quadrilinear backbones. It provides a direct connection between the Static Pushover (SPO) curve and the results of Incremental Dynamic Analysis (IDA), a computer-intensive procedure that offers thorough demand and capacity prediction capability by using a series of nonlinear dynamic analyses under a suitably scaled suite of ground motion records. To achieve this, the seismic behavior of numerous single-degree-of-freedom (SDOF) systems is investigated through IDA. The oscillators have a wide range of periods and feature pinching hysteresis with backbones ranging from simple bilinear to complex quadrilinear with an elastic, a hardening and a negative-stiffness segment plus a final residual plateau that terminates with a drop to zero strength. An efficient method is introduced to treat the backbone shape by summarizing the analysis results into the 16%, 50% and 84% fractile IDA curves, reducing them to a few shape parameters and finding simpler backbones that reproduce the IDA curves of complex ones. Thus, vast economies are realized while important intuition is gained on the role of the backbone shape to the seismic performance. The final product is SPO2IDA, an accurate, spreadsheet-level tool for Performance-Based Earthquake Engineering that can rapidly estimate demands and limit-state capacities, strength reduction *R*-factors and inelastic displacement ratios for any SDOF system with such a quadrilinear SPO curve.

KEY WORDS: performance-based earthquake engineering; incremental dynamic analysis; static pushover; oscillator; nonlinear; strength reduction factor

1. INTRODUCTION

Of great interest in Performance-Based Earthquake Engineering (PBEE) is the accurate estimation of the seismic demand and capacity of structures. To accomplish the task several methods have emerged, a promising one being Incremental Dynamic Analysis (IDA), a parametric analysis method that estimates seismic demand and capacity by subjecting the structural model to several ground motion records,

*Correspondence to: Dimitrios Vamvatsikos, 75 Kallipoleos Str, PO Box 20537, Nicosia 1678, Cyprus.
†E-mail: divamva@stanfordalumni.org
‡Based on a short paper presented at the 7th U.S. National Conference on Earthquake Engineering, Boston, 2002

Contract/grant sponsor: Sponsors of the Reliability of Marine Structures Affiliates Program of Stanford University

Received ? November 2003
Revised 22 April 2004
Accepted 26 January 2006

each scaled to multiple levels of intensity (Vamvatsikos and Cornell [1]). Still, the need for simplified methods for professional practice remains, and the rational choice has often been the use of results stemming from the dynamic analysis of single-degree-of-freedom (SDOF) approximations to the multi-degree-of-freedom (MDOF) structural model. Such methods often use an oscillator with a backbone curve that mimics the Static Pushover (SPO, also known as Nonlinear Static Procedure) curve of the MDOF structure (e.g., FEMA [2]). However, most systematic demand research efforts have not progressed further than using an oscillator with a bilinear backbone, allowing for either positive (e.g., Riddell and Newmark [3], Nassar and Krawinkler [4], Lee *et al.* [5]) or negative (e.g., Al-Sulaimani and Roessett [6], Miranda and Akkar [7]) post-yield stiffness or, still more simply, an elastic perfectly-plastic backbone shape (e.g., Newmark and Hall [8], Vidic *et al.* [9], Miranda [10]), while few, if any, attempts have been made to quantify its dynamic, global-instability collapse capacity. As an extension to existing procedures, we will apply IDA to SDOF systems featuring a variety of backbones and attempt to quantify the resulting demands and capacities in a handful of comparatively simple empirical equations.

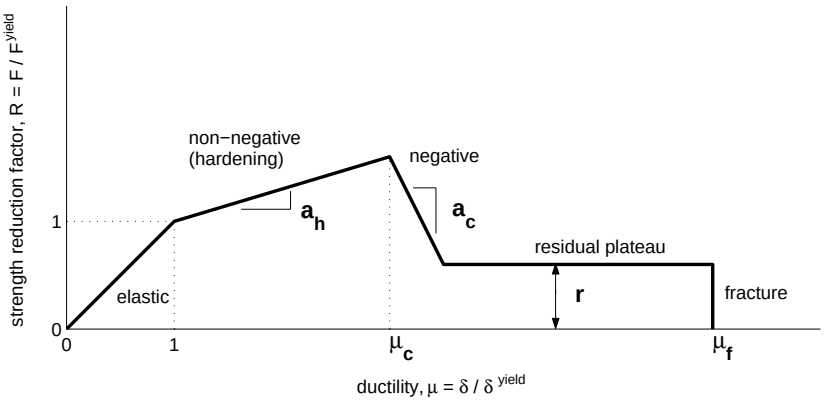

Figure 1. The backbone to be investigated and its five controlling parameters.

2. METHODOLOGY

To study the influence of the SPO curve on the dynamic behavior, we have chosen a piecewise linear backbone that is composed of up to four segments (Figure 1). A full quadrilinear backbone starts elastically, yields at ductility $\mu = 1$ and hardens at a slope $a_h \in [0,1)$, then at ductility $\mu_c \in (1,+\infty)$ it turns negative at a slope $a_c \in [-\infty,0)$, but is revived at $\mu_r = \mu_c + (1-r+(\mu_c-1)a_h)/|a_c|$ by a residual plateau of height $r \in [0,1]$, only to fracture and drop to zero strength at $\mu_f \in [1,+\infty)$. By suitably varying the five parameters, a_h, μ_c, a_c, r and μ_f, almost any (bilinear, trilinear or quadrilinear) shape of the SPO curve may easily be matched.

To fully investigate the dynamic behavior of a single SDOF model, we will use IDA for a suite of thirty ground motion records (Table I) that have been selected to represent a scenario earthquake; the moment magnitude is within 6.5 – 6.9, they have all been recorded on firm soil (USGS type C or B) and show no directivity effects. IDA involves performing a series of nonlinear dynamic analyses for each

Table I. The suite of thirty ground motion records used.

No	Event	Station	ϕ° *	Soil†	M‡	R§ (km)	PGA (g)
1	Loma Prieta, 1989	Agnews State Hospital	090	C,D	6.9	28.2	0.159
2	Northridge, 1994	LA, Baldwin Hills	090	B,B	6.7	31.3	0.239
3	Imperial Valley, 1979	Compuertas	285	C,D	6.5	32.6	0.147
4	Imperial Valley, 1979	Plaster City	135	C,D	6.5	31.7	0.057
5	Loma Prieta, 1989	Hollister Diff. Array	255	–,D	6.9	25.8	0.279
6	San Fernando, 1971	LA, Hollywood Stor. Lot	180	C,D	6.6	21.2	0.174
7	Loma Prieta, 1989	Anderson Dam Downstrm	270	B,D	6.9	21.4	0.244
8	Loma Prieta, 1989	Coyote Lake Dam Downstrm	285	B,D	6.9	22.3	0.179
9	Imperial Valley, 1979	El Centro Array #12	140	C,D	6.5	18.2	0.143
10	Imperial Valley, 1979	Cucapah	085	C,D	6.5	23.6	0.309
11	Northridge, 1994	LA, Hollywood Storage FF	360	C,D	6.7	25.5	0.358
12	Loma Prieta, 1989	Sunnyvale Colton Ave	270	C,D	6.9	28.8	0.207
13	Loma Prieta, 1989	Anderson Dam Downstrm	360	B,D	6.9	21.4	0.24
14	Imperial Valley, 1979	Chihuahua	012	C,D	6.5	28.7	0.27
15	Imperial Valley, 1979	El Centro Array #13	140	C,D	6.5	21.9	0.117
16	Imperial Valley, 1979	Westmoreland Fire Station	090	C,D	6.5	15.1	0.074
17	Loma Prieta, 1989	Hollister South & Pine	000	–,D	6.9	28.8	0.371
18	Loma Prieta, 1989	Sunnyvale Colton Ave	360	C,D	6.9	28.8	0.209
19	Superstition Hills, 1987	Wildlife Liquefaction Array	090	C,D	6.7	24.4	0.18
20	Imperial Valley, 1979	Chihuahua	282	C,D	6.5	28.7	0.254
21	Imperial Valley, 1979	El Centro Array #13	230	C,D	6.5	21.9	0.139
22	Imperial Valley, 1979	Westmoreland Fire Station	180	C,D	6.5	15.1	0.11
23	Loma Prieta, 1989	Halls Valley	090	C,C	6.9	31.6	0.103
24	Loma Prieta, 1989	WAHO	000	-,D	6.9	16.9	0.37
25	Superstition Hills, 1987	Wildlife Liquefaction Array	360	C,D	6.7	24.4	0.2
26	Imperial Valley, 1979	Compuertas	015	C,D	6.5	32.6	0.186
27	Imperial Valley, 1979	Plaster City	045	C,D	6.5	31.7	0.042
28	Loma Prieta, 1989	Hollister Diff. Array	165	–,D	6.9	25.8	0.269
29	San Fernando, 1971	LA, Hollywood Stor. Lot	090	C,D	6.6	21.2	0.21
30	Loma Prieta, 1989	WAHO	090	–,D	6.9	16.9	0.638

* Component † USGS, Geomatrix soil class ‡ moment magnitude §closest distance to fault rupture

record by scaling it to several levels of intensity that are suitably selected to uncover the full range of the model's behavior: elastic, yielding, non-linear inelastic and finally global dynamic instability. Each dynamic analysis can be represented by two scalars, an Intensity Measure (IM), which corresponds to the scaling factor of the record (e.g., the strength reduction factor $R = S_a(T_1,5\%)/S_a^y(T_1,5\%)$, which is equal to the 5%-damped first-mode spectral acceleration $S_a(T_1,5\%)$ normalized by its value that causes first yield) and an Engineering Demand Parameter (EDP), which monitors the structural response of the model (e.g., peak ductility μ).

By suitably interpolating between the runs that were performed for a given record, we can plot on the EDP-IM axes an IDA curve for each record, e.g., Figure 2(a). Each curve ends with a characteristic "flatline" which indicates that the EDP rapidly increases towards "infinite" values for small changes in the IM, thus signalling global dynamic instability and defining the global-collapse capacity at the IM-value where the IDA curve effectively becomes flat. Such "capacity points" are visible as black dots in Figure 2(a). A set of IDA curves can be summarized into 16%, 50% and 84% cross-sectional fractile IDAs of response μ given the intensity R or R given μ, depending on how the cross-sections of the

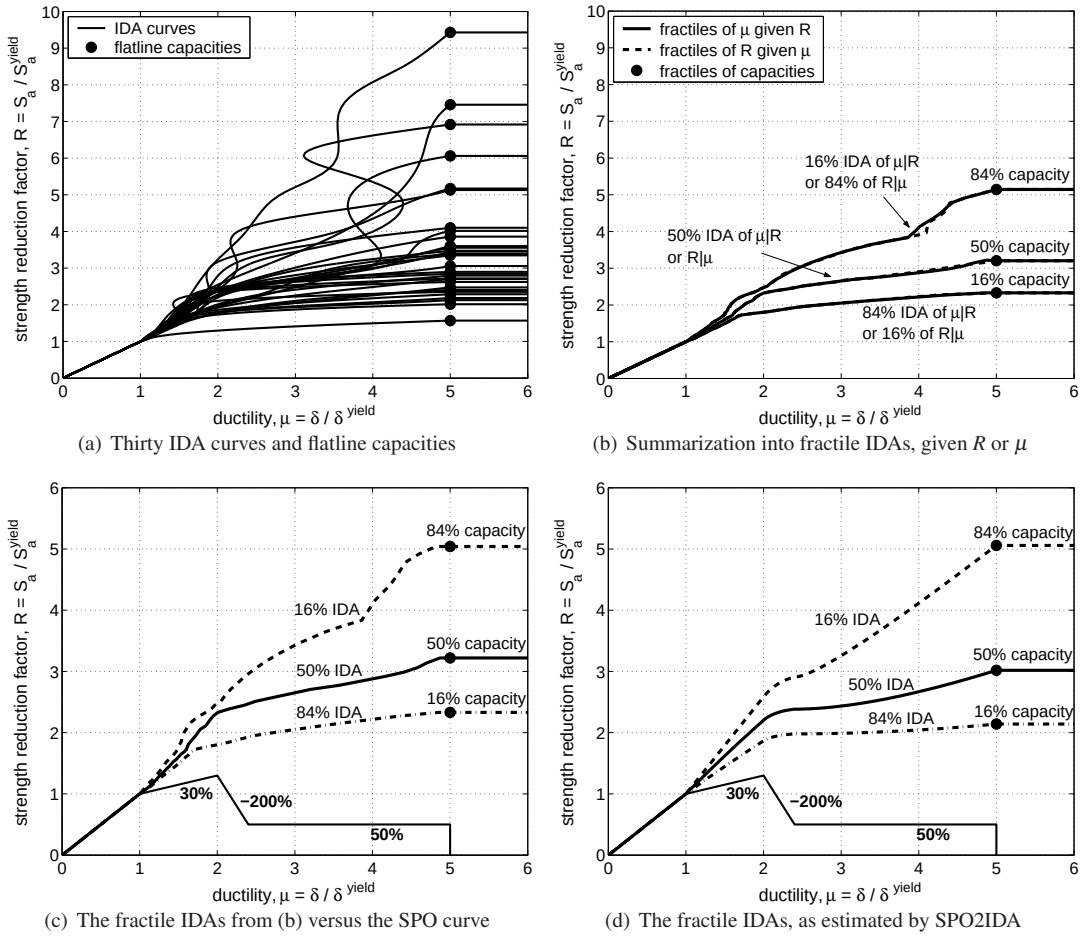

(a) Thirty IDA curves and flatline capacities

(b) Summarization into fractile IDAs, given R or μ

(c) The fractile IDAs from (b) versus the SPO curve

(d) The fractile IDAs, as estimated by SPO2IDA

Figure 2. Generating the fractile IDA curves and capacities from dynamic analyses versus estimating them by SPO2IDA for an SPO with $a_h = 0.3$, $\mu_c = 2$, $a_c = -2$, $r = 0.5$, $\mu_f = 5$.

curves are taken, e.g., at specified levels of R or μ (Vamvatsikos and Cornell [1]). Fortunately, under suitable assumptions of continuity and monotonicity, the $x\%$-fractile IDA $\mu_{x\%}(R)$ ($x \in \{16, 50, 84\}$) of μ given R, will be identical (or nearly identical if the assumptions are slightly violated, Vamvatsikos and Cornell [11]) to the $(100-x\%)$-fractile IDA $R_{(100-x\%)}(\mu)$ of R given μ as shown in Figure 2(b). As a direct result, if we similarly summarize the capacity points, the $(100-x\%)$ global-instability collapse capacity will always appear on the flatline of the $x\%$-fractile IDA of μ given R (Figure 2(c)).

By thus summarizing the fractile IDA curves, we get both a characterization of the distribution of R given μ and μ given R. While the individual IDAs are highly variable and often non-monotonic, i.e., higher values of R do not necessarily correspond to higher values of μ (Vamvatsikos and Cornell [1]), the fractiles are much smoother and empirically are found to be almost always monotonic. They are thus suitable to be modeled with relatively simple functions.

If we plot the SPO of the SDOF system on μ versus $R = F/F^y$ axes (where F is the total base shear

and F^y its value that causes first yield) we can make it appear versus the summarized IDA curves on the same graph (Vamvatsikos and Cornell [1]), as in Figure 2(c). Such a comparison shows that the SPO and the fractiles are composed of the same number of corresponding and distinguishable segments. Moreover, each segment has its own nature. The elastic segment of the SPO naturally coincides with the elastic IDA region for all three fractiles, while the yielding and hardening of the SPO forces the 16%, 84% IDAs to branch uniformly around the median which approximately follows the familiar "equal displacement" rule ($\mu \approx R$) for moderate (and long) periods (Veletsos and Newmark [12]). The SPO's negative stiffness appears as a characteristic flattening of all three IDAs that stops when the residual plateau is activated, causing the "revival" of the IDA curves towards higher R-values. Ultimately, all IDA curves submit to the SPO fracturing and signal collapse by producing a flatline and the corresponding fractile capacity point.

This consistent behavior makes it is possible to approximate each separate segment of the IDA by its prominent features, e.g., the height of the flatline or the slope and intercept of a fitted line. By examining a large enough population of SDOF systems with different backbone shapes, we can track the evolution of the features of each segment, and subsequently model them as a function of the SPO parameters. Thus, we are able to generate almost the same fractile IDAs and capacities (within some acceptable tolerance) without needing to repeat the multiple dynamic analyses. This set of rules and equations will be collectively called the SPO2IDA tool, a typical example of its accuracy visible in Figure 2(d).

However, the complexity of the backbone has forced us to initially limit the scope of our investigation to SDOF systems that share an identical moderately pinching hysteresis model with no cyclic deterioration, developed by Ibarra [13], having $\xi = 5\%$ viscous damping and $T = 0.92$s period. The results will thus be a good approximation for the moderate period range, providing the basis for an extension to short and long periods. Still, the full investigation of a five-dimensional space of parameters requires a staggering amount of dynamic analyses, especially since the parameters do not influence the IDAs independently of each other. Nevertheless, there are several facts that allow us to reduce the size of the problem. First, since we are measuring the *peak* ductility, at any given value of μ the IDA will only be influenced by the segments of the SPO backbone that appear at lower or equal ductilities. This would not be true if we were monitoring, say, permanent deformation. So, in fitting the hardening branch, the negative stiffness is of no consequence, while in fitting the negative branch, the plateau plays no part. Therefore, we can cut the problem into smaller pieces, as we only need to investigate a bilinear elastic-hardening, a trilinear elastic-hardening-negative but still, a full quadrilinear for the plateau. Furthermore, some of the SPO parameters seem redundant, so their influence can be summarized in only one or two new parameters which combine them. Effectively we are going to search for "equivalent backbones" (for the same damping and period), in the sense that such oscillators would share very similar dynamic behavior in the region of interest, as manifested by their displaying the same fractile IDAs.

When modeling the IDA features we will use least-squares fits of polynomials, either in the linear or in the log-domain. To simplify the expressions to follow, we will represent linear combinations of n functions $p_i(y_1,\dots,y_k)$ of given variables $y_1,\dots,y_k$, as a sum $\sum_i b_{x\%,i} p_i(y_1,\dots,y_k)$, where the appropriate functions p_i, $i = 1,\dots,n$, and coefficients $b_{x\%,i}$, (corresponding to the x%-fractile) will be provided in tables.

As a general principle, note that the relatively small number of records, the record-to-record variability and the fitting error, combine to introduce some noise which tends to become larger as the ductility response itself increases. So we will generally fit elaborate models but only as complex as the noise in the IDA results allows. Still, as we try to interpolate as closely as possible given the

noise, we are risking eliciting criticism for "overfitting", in the sense that a simpler model might do only a little worse. The idea is to provide as a complete and objective model as the record-to-record noise allows aiming towards a highly accurate computer tool rather than simplified but less accurate expressions that can be applied by hand.

3. MODERATE PERIOD PINCHING MODEL

3.1. Fitting the hardening branch of the IDA

Fitting the hardening part is the easiest task, and much research exists (e.g., Nassar and Krawinkler [4], Lee *et al.* [5], Miranda [10]), sometimes for a wider variety of parameters (e.g., site conditions, cyclic strength deterioration etc.) than what we will use here. This fit is relatively straightforward as it involves a single parameter, the hardening slope a_h. We will use a second-order polynomial model in the log-space to fit the fractile ductilities given R and then we will fit the resulting coefficients for several values of a_h. Thus, for each of the three fractile IDAs the model becomes

$$\ln \mu_{x\%} = \beta_{x\%} \ln R + \gamma_{x\%} \ln^2 R, \qquad R \in (1, R_{(100-x)\%}(\mu_c)] \tag{1}$$

$$\text{where} \quad \beta_{x\%},\, \gamma_{x\%} = \sum_i b_{x\%,i} p_i(a_h), \quad \text{for any } a_h \in [0, 0.9)$$

where the coefficients and functions can be found in Table II. An example of its application appears in Figure 2(d) for $1 < \mu \leq 2$.

The results are actually only mildly dependant on a_h, especially for low ductilities. So we can roughly approximate the median IDA by the "equal displacement rule", under which $\mu_{50\%}(R) \approx R$, and generate the 16%, 84% fractiles as the edges of a 60%-wide band centered on the median (in the log-space), i.e., $\mu_{(50\pm34)\%}(R) \approx \mu_{50\%}(R)^{1\pm0.3} \approx R^{1\pm0.3}$.

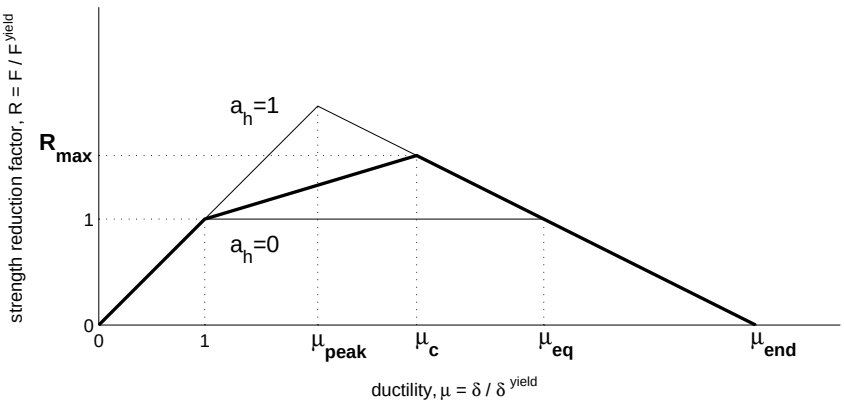

Figure 3. An elastic-hardening-negative backbone and the two extremes of its "equivalent" set.

3.2. Fitting the negative branch of the IDA

Negative stiffness is found in SPOs of structures such as non-ductile reinforced-concrete frames, braced steel frames, moment-resisting steel frames with fracturing connections and P-Δ sensitive systems.

The most prominent feature of the negative branch is the characteristic flattening of the summarized IDAs which results in a flatline unless it is arrested by the residual plateau, as seen in Figure 2(c), for $2 < \mu \leq 2.4$. By accurately capturing this feature, the entire branch could be modeled as a continuous convex curve that smoothly departs from the hardening segment at ductility μ_c to blend into the flatline at $\mu_{\text{end}} = \mu_c + (1 + a_h\mu_c - a_h)/|a_c|$. Still, appropriately modeling the negative branch flatline requires a trilinear (elastic-hardening-negative) backbone that involves three independent parameters (a_c, a_h and μ_c). It was found empirically that this flatline height and, even more, the complete negative part of the IDA are very similar for the set of backbones that have coincident negative branches, like those in Figure 3. Actually, the flatline height among such an equivalent set varies only a little and always in a consistent linearly increasing fashion between the two extremes, i.e., the $a_h = 0$ and the $a_h = 1$ cases where the negative branch starts at $\mu_{\text{eq}} = \mu_c + a_h(\mu_c - 1)/|a_c|$, and $\mu_{\text{peak}} = (\mu_c|a_c| + 1 + a_h(\mu_c - 1))/(1 + |a_c|)$ respectively. So we only need to model the capacities for the extreme values of a_h and linearly interpolate in-between. The final recommended model becomes:

$$R_{(100-x)\%}(\mu_{\text{end}}) = R_{(100-x)\%}(\mu_c) + \left(e^{\beta_{x\%}} - 1\right)\left[l^{\text{eq}}_{(100-x)\%} + a_h\left(\mu_{\text{peak}} - l^{\text{eq}}_{(100-x)\%}\right)\right], \tag{2}$$

$$l^{\text{eq}}_{(100-x)\%} = (\mu_{\text{eq}})^{\gamma_{x\%}}, \tag{3}$$

$$\text{where} \quad \beta_{x\%}, \gamma_{x\%} = \sum_i b_{x\%,i} p_i(a_c), \qquad \text{for any } a_c \in [-4, -0.01],\ a_h \in [0,1),\ \mu_c \in [1,9]$$

where the coefficients are found in Table II.

As a first, simpler approximation for moderate values of the negative slope a_c, one may assume that in log-space the 16% and 84% flatlines are roughly 30%-lower and 30%-higher than the median, i.e., $R_{(50\pm34)\%}(\mu_{\text{end}}) = R_{50\%}(\mu_{\text{end}})^{1\pm0.3}$.

3.3. Fitting the residual part of the IDA

The residual plateau in the SPO is encountered, for example, in braced frames or fracturing moment-resisting frames. Only limited inspection of such models has appeared in the literature (e.g., Stear and Bea [14]). The SPO residual plateau allows the IDA to escape the negative-branch flattening and move to higher R-values in an almost linear fashion, e.g., Figure 2(c) for $3 < \mu < 5$. We can model this feature by a linear segment in log-space and capture this entire IDA region by a continuous convex curve that smoothly rises from the negative-branch flattening. This would depend on all five backbone parameters but for the empirical finding that, in this region of the IDA, the full quadrilinear model displays virtually the same behavior as an equivalent trilinear (elastic-negative-plateau) model that has the same negative slope a_c and a reduced plateau height of $r_{\text{eq}} = r/(1 + a_h(\mu_c - 1))$. Actually, r_{eq} is the residual plateau height of the full model but measured relative to the peak R-value, $R_{\max} = 1 + a_h(\mu_c - 1)$, reached by the SPO (Figure 3), instead of relative to the yield strength. This leaves only two parameters, a_c and r_{eq}, resulting in the model:

$$\ln \mu_{x\%} = \beta_{x\%} + \gamma_{x\%} \ln R, \qquad R \in \left(R_{(100-x)\%}(\mu_r), R_{(100-x)\%}(\mu_f)\right] \tag{4}$$

$$\text{where} \quad \beta_{x\%},\ \gamma_{x\%} = \sum_i b_{x\%,i} p_i\left(a_c, r_{\text{eq}}\right),\ \text{for any } a_c \in [-4, -0.01], \quad r_{\text{eq}} \in [0.05, 0.90]$$

where the coefficients can be found in Table II. An example of this model's application can be seen in Figure 2(d) for $3 < \mu \leq 5$.

By observing the results, one can derive that the median IDA does behave much like a secant linear segment that takes on smaller slopes as r_{eq} decreases, eventually becoming one with the flatline induced

Table II. Coefficients and functions needed for fitting the IDA hardening, negative and residual parts in Equations (1), (2), (4).

	$b_{x\%,i}$ for $\beta_{x\%}$				$b_{x\%,i}$ for $\gamma_{x\%}$		
hardening	16%	50%	84%		16%	50%	84%
1	0.6164	0.7132	1.0024		0.1454	0.2928	0.4003
a_h	-0.1697	-0.0415	1.5907		-0.1394	-0.6415	-3.0742
$(a_h)^2$	1.3103	1.5158	-7.1722		-0.2576	0.0347	9.7763
$(a_h)^3$	-1.9551	-2.5525	10.3472		0.6156	0.9604	-12.8813
$(a_h)^4$	1.2201	1.3921	-4.8024		-0.3707	-0.6620	5.8376
negative	16%	50%	84%		16%	50%	84%
1	0.2252	0.3720	0.6130	$\lvert a_c\rvert^{-1}$	-0.5111	-0.3817	-0.4118
$\ln\lvert a_c\rvert$	-0.1850	-0.3023	-0.4392	1	-0.6194	-0.3599	-0.2610
$\ln^2\lvert a_c\rvert$	0.1039	0.1056	0.0847	$\lvert a_c\rvert$	0.0928	-0.0019	-0.0070
				$\lvert a_c\rvert^2$	0.0163	0.0186	0.0158
residual	16%	50%	84%		16%	50%	84%
1	-0.3615	0.2391	0.9557		1.1022	1.0846	1.0176
$\ln\lvert a_c\rvert$	-0.0729	-0.0297	-0.0696		0.0180	0.0081	0.0203
$\ln r_{\text{eq}}$	-0.4557	-0.4907	-0.4759		0.1111	0.1218	0.1086
$\ln r_{\text{eq}} \cdot \ln\lvert a_c\rvert$	-0.0372	-0.0272	-0.0308		0.0136	0.0086	0.0061

by the negative branch of the SPO. So, by restricting ourselves to (quite practical) ductilities of 10 or less, we could model the residual branch of the median IDA as a secant by assuming $\gamma_{50\%} = 1$, while generating the 16%, 84% fractiles as a 100%-wide band centered on the median (in log-space), i.e., $\mu_{(50\pm34)\%}(R) \approx \mu_{50\%}(R)^{1\pm0.5} \approx \beta_{50\%} \cdot R^{1\pm0.5}$. The existing $\beta_{50\%}$ coefficients are not optimal but can still be used for this rough approximation.

3.4. Joining the pieces: The SPO2IDA tool

We have separately modeled the three segments and we have chosen to keep track of only the flattening caused by the negative SPO and the "secant" caused by the residual. To join them into smooth and continuous curves that accurately resemble the fractile IDAs we need two "filleting curves" that will connect the negative branch flatline to the hardening and the "secant". A simple but less accurate method is to linearly extend all three separate segments to a point of mutual interception. Alternatively, we can generate splines through a knot-insertion algorithm (Farin [15]), which provides a smooth transition from segment to segment, while at the same time offering computational simplicity and robustness, as it preserves convexity and can be made to be monotonic (as the fractile IDAs are empirically known to be). Thus, we gain an almost complete description of the IDA for any ductility, modeled as an invertible one-to-one function of either μ or R, an advantage of the equivalency of the fractiles given R or μ. We are only missing the flatline, caused by the SPO's ending at ductility μ_f. This can be accurately modeled by adding a flatline to the IDAs at $R_{(100-x)\%}(\mu_f)$, simultaneously producing the $(100-x)\%$-fractile of global-collapse capacity. By implementing in software the modeling and joining of the IDA segments, a process explained in more detail by Vamvatsikos [16], we have generated the SPO2IDA tool. It is free-source program, available as a spreadsheet [17] or an internet application [18], that accurately reproduces the behavior of oscillators, as Figure 2(d) demonstrates.

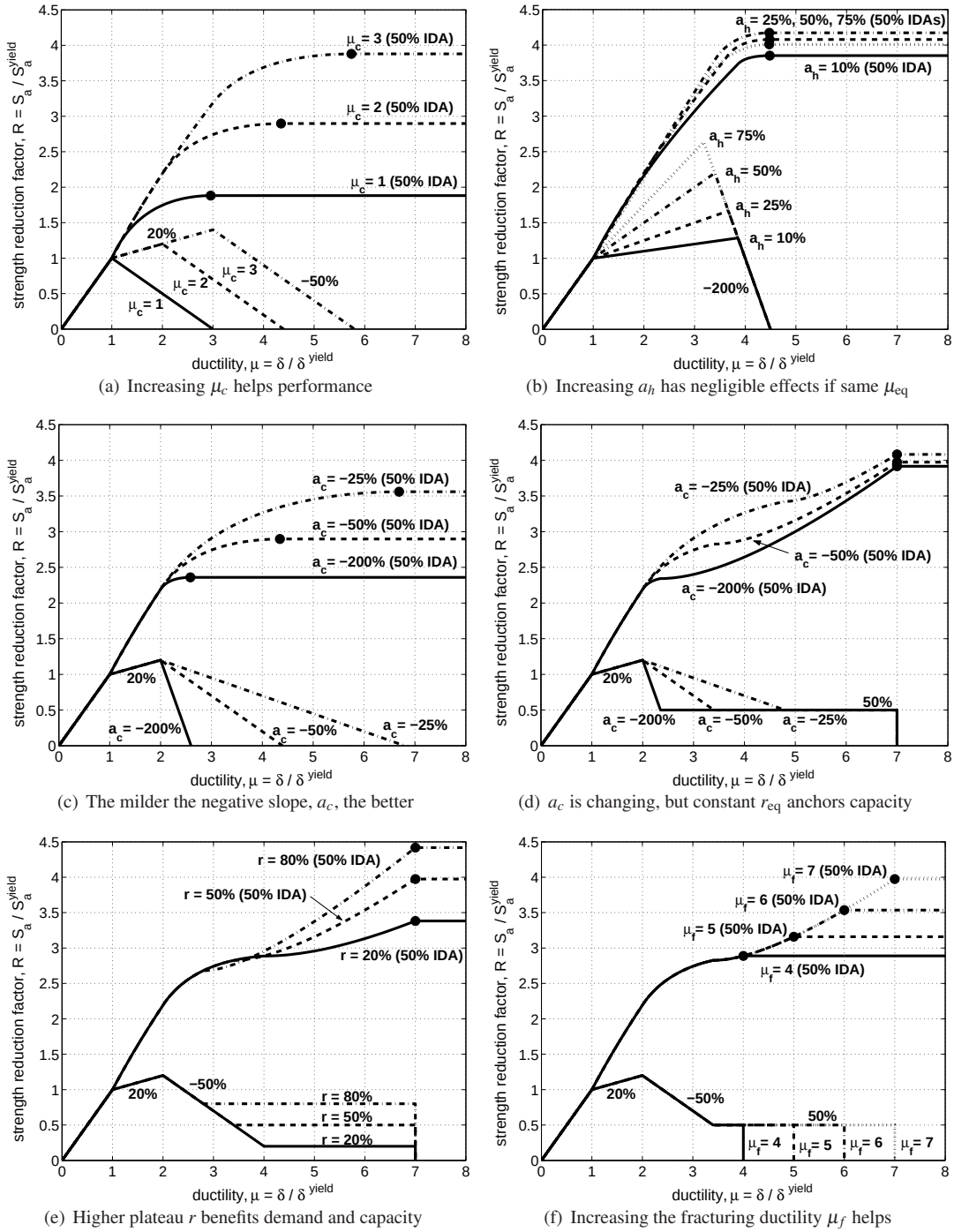

(a) Increasing μ_c helps performance

(b) Increasing a_h has negligible effects if same μ_{eq}

(c) The milder the negative slope, a_c, the better

(d) a_c is changing, but constant r_{eq} anchors capacity

(e) Higher plateau r benefits demand and capacity

(f) Increasing the fracturing ductility μ_f helps

Figure 4. Demonstrating SPO2IDA: the median demand and collapse capacity as the SPO changes.

3.5. *Illustrative Results and Observations*

The ease of computation provided by such a tool, plus the unique perspective offered by the IDA-versus-SPO picture, can offer remarkable intuition into the seismic behavior of systems. As a demonstration of the SPO2IDA tool we present Figure 4, an array of cases to briefly study the influence of the backbone on the seismic demand and capacity. In each figure we select a basic backbone, vary one or two of its parameters and then generate the median IDA responses and the corresponding global instability collapse-capacities for each case. Figure 4(a) shows the benefit of delaying the negative branch of the SPO and allowing hardening to reach higher ductilities. Each increase in μ_c allows the median to stay on "equal displacement" longer, proportionally increasing the capacity. On the other hand, in Figure 4(b), radically changing the hardening slope a_h but keeping an identical negative branch generates an equivalent set of trilinear SPOs, whose capacities only slightly increase with a_h. Actually, the difference in the capacity is small enough to be within the noise in the fitted data, so the resulting capacities are not strictly increasing with a_h. Decreasing the negative slope a_c in Figure 4(c) has a beneficial effect when no residual plateau is present, as the milder slopes allow higher capacities. Still, if we include an extensive enough residual plateau (Figure 4(d)), the benefits of the milder slope are restricted to the somewhat lower μ-demands that may influence some earlier limit-states; the global instability collapse capacity is almost the same for all cases, as the backbones have the same r_{eq}, therefore the milder a_c's are providing only a small advantage. Figure 4(e) shows the benefits of increasing the residual plateau that consequently increases the slope of the "secant" that the IDA follows, thus improving capacities and decreasing the demands. And finally, Figure 4(f) shows the obvious advantage of allowing higher fracturing ductilities μ_f. The value of μ_f literally decides where to terminate the IDA, at times fully negating the effect of the plateau if it becomes too small; at $\mu_f = 4$ the IDA hardly receives any benefit from the plateau. As intuitive or surprising as some of the pictures in Figure 4 may be, they are only a glimpse of what our new tool can really do.

3.6. *SPO2IDA error estimates for moderate periods*

Since the SPO2IDA tool is based on fitting over only a small subset of the SDOF backbones it can simulate, just showing the fitting error over the sample of oscillators that we have used would greatly underestimate the true prediction error. In order to be objective we have generated a large separate test sample of randomly chosen bilinear, trilinear and quadrilinear backbones that were analyzed both through full IDA and SPO2IDA. Thus, for each backbone and each of the three $x\%$-fractiles we are presented with two IDA curves, the "real" curve $R_{(100-x)\%}(\mu)$ and the approximate $\hat{R}_{(100-x)\%}(\mu)$, or equivalently expressed in μ given R coordinates, $\mu_{x\%}(R)$ versus $\hat{\mu}_{x\%}(R)$.

We are interested in knowing the error in two different settings: error in estimating a demand μ given a certain level on intensity R and error in estimating a capacity R given a certain level of demand μ. In both cases, the *absolute* difference between exact and approximate results tends to increase rapidly when we progress further into the nonlinear range, making this measure unsuitable. We choose instead to quantify the errors by integrating the *relative absolute* difference of each approximate $x\%$-fractile IDA curve versus the real one over their length, either in μ or R coordinates accordingly, a concept similar to the one used by Lee *et al.* [5]:

$$(\varepsilon_R)_{x\%} = \int_0^{\mu_f} \frac{\left|R_{(100-x)\%}(\mu) - \hat{R}_{(100-x)\%}(\mu)\right|}{R_{(100-x)\%}(\mu)}\,\mathrm{d}\mu \tag{5}$$

$$(\varepsilon_\mu)_{x\%} = \int_0^{R_f} \frac{\left|\mu_{x\%}(R) - \hat{\mu}_{x\%}(R)\right|}{\mu_{x\%}(R)}\,\mathrm{d}R \tag{6}$$

Table III. Average fractile-demand and fractile-capacity errors for moderate periods and a variety of backbone shapes, as caused by the fitting in SPO2IDA and by the record-to-record variability and limited record suite size in IDA.

	SPO2IDA			10 records			30 records		
$x\% =$	16%	50%	84%	16%	50%	84%	16%	50%	84%
elastic-hardening									
ε_R	0.02	0.01	0.02	0.11	0.07	0.07	0.06	0.04	0.04
ε_μ	0.01	0.01	0.02	0.06	0.06	0.09	0.04	0.03	0.05
elastic-hardening-negative									
ε_R	0.02	0.03	0.03	0.09	0.06	0.06	0.05	0.03	0.03
ε_μ	0.02	0.03	0.03	0.07	0.05	0.06	0.04	0.03	0.04
elastic-hardening-negative-plateau									
ε_R	0.16	0.14	0.18	0.20	0.12	0.13	0.12	0.08	0.07
ε_μ	0.09	0.11	0.18	0.20	0.18	0.23	0.11	0.11	0.14

In each case, the fractile-capacity error $(\varepsilon_R)_{x\%}$ is calculated over the full demand spectrum from zero to μ_f, and the fractile-demand error $(\varepsilon_\mu)_{x\%}$ is similarly calculated up to R_f, the earliest flatline of the compared curves.

What is more important to the user is an assessment of SPO2IDA's estimation error, caused by imperfect fitting, as compared to the full IDA estimation error caused by the record-to-record variability when using a limited sample of records. To provide such a standard for comparison, we will use the bootstrap method (Efron and Tibshirani [19]) to estimate the $(\varepsilon_R)_{x\%}$ and $(\varepsilon_\mu)_{x\%}$ errors that one would expect to encounter when using only 10 or 30 randomly chosen records from the same scenario earthquake. The original 30 records are sampled with replacement to generate numerous alternate samples of 10 and 30 records, which are then applied to each of the randomly-chosen backbones, thus resulting to a large number of alternate estimates of the fractile IDAs for each test-case. Then, using the original 30-record suite results as "exact", the average (over all bootstrap samples) $(\varepsilon_R)_{x\%}$ and $(\varepsilon_\mu)_{x\%}$ are calculated, as shown in Table III.

Before we interpret these results, it is important to understand that SPO2IDA was based on the 30-record IDA, thus its error, as calculated in the table, comes *in addition* to the error induced by the record-to-record variability in the 30-record fractile IDAs, i.e., SPO2IDA cannot be more accurate than a 30-record IDA. Still, if the additional (fitting induced) error it incurs is small enough, it will disappear (as when taking the square root of sum of squares of the two errors) under the considerable (record-variability induced) error in estimating the fractiles with a 30-record IDA. Thus, by comparing the $(\varepsilon_R)_{x\%}$ and $(\varepsilon_\mu)_{x\%}$ of SPO2IDA versus the average such errors due to the record-to-record variability, we observe that SPO2IDA can estimate the fractile demands or capacities with an error comparable to the record-to-record noise around the 10-record full IDA results. This means that, statistically, the difference between the full IDA and SPO2IDA results is on average insignificant when only 10 records are used. If 30 records are employed for IDA, SPO2IDA again performs very well for all backbones except the complex quadrilinears where it has, on average, an error somewhat more significant, but still comparable to the record-to-record induced noise. All in all, SPO2IDA is proven to be remarkably accurate, able to outperform the 10-record full IDA and in many cases match the 30-record IDA.

The values in Table III only describe the performance of SPO2IDA averaged over numerous

backbone shapes and over the length (either in R or μ terms) of the fractile curves. Some individual backbone shapes may be captured better than others and within the curves themselves some segments may be more accurately matched. As evident from Table III, the error tends to increase for more complex backbones, partly due to the cascading of the models; as more segments are added to the backbone, each additional segment relies on the accuracy achieved in the previous ones. Thus, we should expect higher error in the later segments (e.g., the residual plateau). Even within the same segment of the curve, the distribution of the error is not homogeneous, neither for the full IDA, nor for the SPO2IDA. In the IDA results, as the ductility increases beyond yielding, the record-to-record variability and the error it induces increase as well. This, in turn, introduces higher noise in the fitted data, thus making the fitted equations less accurate at higher ductilities. So, in general, one should expect errors lower than average at low ductilities and higher than average at high ductilities for both methods. Finally, since we have used regression to fit the IDA curves, these equations will perform better in the middle of the fitted dataset and worse at the edges (Weisberg [20]). So, one should generally expect higher errors closer to the edges, e.g., at $a_c = -0.01$ for Equation 2 or at $r_{\text{eq}} = 0.9$ and $a_c = -0.01$ in Equation 4. In conclusion, there are combinations of backbone parameters that may cause SPO2IDA to produce a mediocre estimate for some segment of the IDA, but in our experience even these cases are rare.

4. EXTENSION TO ALL-PERIODS PINCHING MODEL

Up to now we have described a procedure used to obtain the fractile IDA curves of a fairly limited model. Still, this can be easily extended to other periods, dampings, or hysteretic models. What we have really introduced above is a methodology that permits the accurate modeling of the SDOF fractile IDA curves for complex backbones by investigating only a small number of them. If one wishes to capture the behavior of a different SDOF system, or use a different suite of ground motion records, all that is needed is repeating the above three fits for the hardening, negative and residual part to include the new parameters. As an example, we are going to extend SPO2IDA to both short and long periods, still using the same suite of 30 records, moderately pinching hysteresis and viscous damping of $\xi = 5\%$. The overall concept will be precisely the same as for the moderate periods, simply the necessary coefficients will be given by more complicated equations that, in addition to the backbone parameters, will now include the oscillator period T.

Unfortunately, the period influences each of the backbone regions in a complex, coupled way, that makes it impossible to assume independence. So, where we had mostly one or two dimensional fits, now we will have two and three dimensional ones. This fact increases the number of oscillators that we have to investigate by an order of magnitude. Still, the fundamental results that we previously employed to reduce the number of backbones investigated are not period dependent. For example, when fitting the flatline heights induced by the negative branch, although for non-moderate periods they may vary significantly within an "equivalent" set, they are still found to depend linearly on a_h.

4.1. Fitting the hardening, negative and residual branch of the IDA

We can use Equations (1)–(4) that accurately capture the features of the corresponding part of the IDA; we only need to provide fits for the coefficients $\beta_{x\%}$ and $\gamma_{x\%}$ that include dependance on T:

$$\ln \beta_{x\%} = \sum_i b_{x\%,i}\, p_{x\%,i}(a_h, T), \quad \ln(\gamma_{x\%} + 1) = \max\left(\sum_i b_{x\%,i}\, p_i(a_h, T)\,, 0\right), \tag{7}$$

$$\text{for any } a_h \in [0, 0.9], T \in [0.2\text{s}, 4\text{s}]$$

$$\beta_{x\%} = \sum_i b_{x\%,i} p_i(a_c, T), \qquad \gamma_{x\%} = \min\left(\sum_i b_{x\%,i} p_i(a_c, T), 1\right) \tag{8}$$

$$\text{for any } a_c \in [-4, -0.02],\ T \in [0.2\text{s}, 4\text{s}]$$

$$\beta_{x\%},\ \gamma_{x\%} = \sum_i b_{x\%,i} p_i(a_c, r_{\text{eq}}, T), \tag{9}$$

$$\text{for any } a_c \in [-4, -0.05], \quad r_{\text{eq}} \in [0.05, 0.90], \quad T \in [0.2\text{s}, 4\text{s}]$$

The coefficients $b_{x\%,i}$ and corresponding functions can be found in Table IV for the hardening (Equation 7), the negative (Equation 8) and the residual (Equation 9) part of the IDA curves.

As expected, the results are relatively similar in the moderate and long period range especially for the hardening branch where the median is predictably following the "equal displacement" rule; even there the situation is much different in the short period domain. In that region there is significant dependance on T, making any simplifications of the above equations quite difficult.

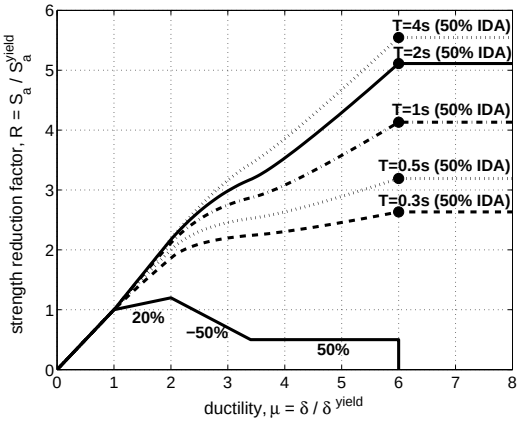

Figure 5. Median IDAs for a backbone with $a_h = 0.2$, $\mu_c = 2$, $a_c = -0.5$, $r = 0.5$, $\mu_f = 6$ but varying periods.

4.2. Illustrative Results and Observations

Using splines to connect the above presented three fits and to integrate them into SPO2IDA, we have generated a tool that can accurately capture the behavior of a complex quadrilinear backbone for a wide range of periods, from 0.2s to 4s (Vamvatsikos [21]). An example of its application is presented in Figure 5. Therein the median IDA curve of an elastic-hardening-negative-plateau backbone is recreated for several oscillator periods. Starting at a moderate period of $T = 1$s, the flatline happens at $R \approx 4.1$, but if we decrease the period down to $T = 0.3$s, we observe that the IDA becomes more aggressive; softening commences at very low values of R and the flatline is reached very quickly, at $R \approx 2.7$ for $T = 0.3$s. On the other end, when the period is increased, the median IDA is "milder", it rises and straightens out, staying longer on the "equal displacement" rule, i.e., on the $\mu = R$ line. Thus, the flatline is greatly delayed, occurring at $R \approx 5.5$ at $T = 4$s. Obviously, the oscillator period has a significant effect on the flatline but also on all the features of the fractile IDAs. The only exception

Table IV. Coefficients needed for fitting the IDA hardening, negative and residual part in Equations (7)–(9).

	$b_{x\%,i}$ for $\beta_{x\%}$				$b_{x\%,i}$ for $\gamma_{x\%}$		
hardening	16%	50%	84%		16%	50%	84%
$\ln^{-1}(T+1)$	-0.1520	-0.1985	-0.6344		0.1925	0.3689	0.9434
1	-0.5027	-0.0955	0.2649		0.1246	0.0480	0.0277
$\ln T$	-0.0542	-0.0316	0.0818		-0.1045	-0.1747	-0.4226
$\ln^2 T$	0.0181	0.0291	-0.1250		0.0605	0.1364	0.3241
$a_h \ln^{-1}(T+1)$	-0.1520	-0.1985	-0.6344		0.1925	0.3689	0.9434
a_h	0.8058	0.3737	-0.0954		-0.1989	-0.2105	-0.0297
$a_h \ln T$	0.2037	0.2334	0.5720		-0.0822	-0.1916	-0.5081
$a_h \ln^2 T$	-0.2572	-0.3683	-0.5508		0.1711	0.3816	0.5662
$\sqrt{a_h} \ln^{-1}(T+1)$	-0.1520	-0.1985	-0.6344		0.1925	0.3689	0.9434
$\sqrt{a_h}$	-0.3675	-0.3041	-0.1600		0.0713	0.1533	-0.0010
$\sqrt{a_h} \ln T$	-0.1520	-0.1985	-0.6344		0.1925	0.3689	0.9434
$\sqrt{a_h} \ln^2 T$	0.2258	0.3128	0.6418		-0.2237	-0.4964	-0.8851
negative	16%	50%	84%		16%	50%	84%
1	0.2391	0.3846	0.5834	1	-0.2508	-0.2762	-0.2928
$\ln T$	0.0517	0.0887	0.1351	$\lvert a_c \rvert$	-0.5517	-0.1992	-0.4394
$\ln \lvert a_c \rvert$	-1.2399	-1.3531	-1.4585	a_c^2	0.0941	-0.0031	0.0683
$\ln \lvert a_c \rvert \ln T$	-0.0976	-0.1158	-0.1317	$\lvert a_c \rvert^{-1}$	0.0059	0.0101	0.0131
$\ln^2 \lvert a_c \rvert$	0.0971	0.1124	0.1100	$\ln T$	0.1681	0.2451	0.1850
$\ln^2 \lvert a_c \rvert \ln T$	0.0641	0.0501	0.0422	$\lvert a_c \rvert \ln T$	0.1357	-0.0199	0.1783
$\ln^3 \lvert a_c \rvert$	-0.0009	0.0041	0.0056	$a_c^2 \ln T$	-0.0127	0.0091	-0.0305
$\ln^3 \lvert a_c \rvert \ln T$	0.0072	0.0067	0.0074	$\lvert a_c \rvert^{-1} \ln T$	0.0010	-0.0075	-0.0066
				$\ln^2 T$	-0.1579	-0.0135	0.0027
				$\lvert a_c \rvert \ln^2 T$	0.2551	-0.0841	0.0447
				$a_c^2 \ln^2 T$	-0.0602	0.0222	-0.0151
				$\lvert a_c \rvert^{-1} \ln^2 T$	0.0087	-0.0003	-0.0025
residual	16%	50%	84%		16%	50%	84%
1	-0.2226	0.1401	0.7604		1.0595	1.0635	1.0005
$\ln \lvert a_c \rvert$	-0.0992	-0.0817	-0.1035		0.0236	0.0177	0.0283
$\ln r_{\text{eq}}$	-0.4537	-0.5091	-0.5235		0.1237	0.1466	0.1607
$\ln r_{\text{eq}} \cdot \ln \lvert a_c \rvert$	-0.0398	-0.0236	-0.0287		0.0111	0.0048	-0.0004
$\ln r_{\text{eq}}^{-1}$	0.0829	-0.0364	-0.0174		-0.0023	0.0102	0.0021
$\ln r_{\text{eq}}^{-1} \cdot \ln \lvert a_c \rvert$	0.0193	-0.0126	-0.0118		0.0008	0.0019	0.0035
$\ln T$	-0.1831	-0.2732	-0.5651		-0.0881	-0.1044	-0.1276
$\ln T \cdot \ln \lvert a_c \rvert$	-0.0319	0.0015	0.0437		-0.0077	-0.0137	-0.0413
$\ln T \cdot \ln r_{\text{eq}}$	0.1461	0.1101	0.0841		-0.0239	-0.0090	-0.0085
$\ln T \cdot \ln r_{\text{eq}} \cdot \ln \lvert a_c \rvert$	-0.0227	-0.0045	0.0159		0.0025	-0.0014	-0.0198
$\ln T \cdot \ln r_{\text{eq}}^{-1}$	-0.0108	0.0333	0.0033		0.0082	-0.0003	0.0037
$\ln T \cdot \ln r_{\text{eq}}^{-1} \cdot \ln \lvert a_c \rvert$	-0.0081	-0.0000	0.0033		0.0007	-0.0013	-0.0043
$\ln^2 T$	0.1660	0.1967	0.0929		0.0317	0.0038	0.0673
$\ln^2 T \cdot \ln \lvert a_c \rvert$	-0.0124	-0.0304	0.0130		0.0006	0.0065	0.0074
$\ln^2 T \cdot \ln r_{\text{eq}}$	0.0273	0.0396	0.0580		-0.0173	-0.0484	-0.0737
$\ln^2 T \cdot \ln r_{\text{eq}} \cdot \ln \lvert a_c \rvert$	-0.0167	-0.0209	-0.0144		0.0056	0.0068	0.0255
$\ln^2 T \cdot \ln r_{\text{eq}}^{-1}$	-0.0182	0.0311	0.0221		0.0007	-0.0112	-0.0073
$\ln^2 T \cdot \ln r_{\text{eq}}^{-1} \cdot \ln \lvert a_c \rvert$	-0.0097	-0.0047	0.0007		0.0004	0.0008	0.0005

Table V. Average fractile-demand and fractile-capacity errors for short, moderate and long periods and a variety of backbone shapes, as caused by the fitting in SPO2IDA and by the record-to-record variability and limited record suite size in IDA.

	SPO2IDA			10 records			30 records		
$x\% =$	16%	50%	84%	16%	50%	84%	16%	50%	84%
elastic-hardening									
ε_R	0.04	0.04	0.05	0.09	0.07	0.09	0.06	0.04	0.05
ε_μ	0.02	0.03	0.04	0.06	0.06	0.09	0.04	0.04	0.06
elastic-hardening-negative									
ε_R	0.05	0.04	0.05	0.08	0.06	0.09	0.05	0.04	0.04
ε_μ	0.05	0.03	0.04	0.07	0.07	0.10	0.04	0.04	0.04
elastic-hardening-negative-plateau									
ε_R	0.20	0.18	0.20	0.21	0.16	0.18	0.14	0.10	0.12
ε_μ	0.19	0.24	0.26	0.20	0.17	0.24	0.12	0.12	0.15

appears for moderate and long periods in the region where the backbone is still hardening. There the median IDA follows the equal displacement rule and thus becomes insensitive to the (moderate or long) period. As observed at least for the median in Figure 5, SPO2IDA is now able to capture all such period-dependent effects.

4.3. SPO2IDA error estimates for all periods

Similarly to the moderate period model, we have generated a separate test-sample of various oscillators with randomly generated backbones and periods. Then we calculated the fractile demand and capacity errors $(\varepsilon_\mu)_{x\%}$ and $(\varepsilon_R)_{x\%}$ according to Equations (5)–(6) both shown in Table V. Therein we have also included the bootstrapped $(\varepsilon_\mu)_{x\%}$ and $(\varepsilon_R)_{x\%}$ values for a full IDA with 10 and 30 records.

Once again, the SPO2IDA error is, practically speaking, comparable to the error induced by the record-to-record variability in a full 30-record IDA for all cases, except the last, the quadrilinear one. Same as before, the most complex backbone shapes are harder to capture, but still, the SPO2IDA error remains within reasonable limits. Similarly to the moderate period case, the errors in Table V are averaged over numerous backbones, periods and along each individual fractile curve. Therefore, individual cases may perform better or worse than the posted values. The only difference from the moderate period case is the additional consideration of period. Generally, in the short period range, the record-to-record variability is higher thus degrading the accuracy of both IDA and SPO2IDA. Still, barring some isolated below-average-accuracy estimates, the results are very reliable.

5. FROM THE IDA TO THE INELASTIC DISPLACEMENT RATIOS

On a more practical aspect, SPO2IDA can directly produce R-factors and inelastic displacement ratios, often used in seismic guidelines (e.g., FEMA [2]). The direct mapping of the μ-given-R to the R-given-μ fractiles effortlessly provides fractile R-factors. Similarly, one can easily generate $(C_\mu)_{x\%}$, the $x\%$-fractile of inelastic to elastic displacement ratio given μ, and $(C_R)_{x\%}$, the $x\%$-fractile of inelastic to elastic displacement ratio given R, as defined in Miranda [22]. Actually the fractiles of the two

ratios are equivalent as $(C_\mu)_{x\%} = (C_R)_{x\%} = \mu_{x\%}(R)/R = \mu/R_{(100-x)\%}(\mu)$. By modeling the fractiles in SPO2IDA we can use the same fits to generate the R-factors and both the inelastic displacement ratios; had we chosen to model the mean response, we would need a separate fit for each of the three quantities (Miranda [22]).

On the other hand, instead of the fractiles, the mean R-factors or mean inelastic displacement ratios may be of interest. If $E[\cdot]$ is the expectation operator, then we want to estimate $E[R]$, $E[C_\mu] = \mu E[1/R]$ for a given value of μ and $E[C_R] = E[\mu]/R$ for a given value of R. Actually, for values of R higher than any of the flatlines, $E[\mu]$ and correspondingly $E[C_R]$ become infinite. At lower R-values the distribution of μ given R is approximately lognormal (Shome and Cornell [23]) and so is the distribution of R given μ for *any* μ-value. In those ranges we can use the properties of the lognormal distribution (e.g., Benjamin and Cornell [24]) to show that

$$E[R] = R_{50\%}(\mu)\cdot\exp\left(\frac{1}{2}\sigma^2_{\ln R}\right), \qquad \sigma_{\ln R} = \frac{1}{2}\left(\ln R_{84\%}(\mu) - \ln R_{16\%}(\mu)\right) \tag{10}$$

$$E[C_R] = \frac{E[\mu]}{R} = \frac{\mu_{50\%}(R)}{R}\cdot\exp\left(\frac{1}{2}\sigma^2_{\ln \mu}\right), \qquad \sigma_{\ln \mu} = \frac{1}{2}\left(\ln \mu_{84\%}(R) - \ln \mu_{16\%}(R)\right) \tag{11}$$

$$E[C_\mu] = \mu E\left[\frac{1}{R}\right] = \frac{\mu}{R_{50\%}(\mu)}\cdot\exp\left(\frac{1}{2}\sigma^2_{-\ln R}\right), \qquad \sigma_{-\ln R} = \sigma_{\ln R} \tag{12}$$

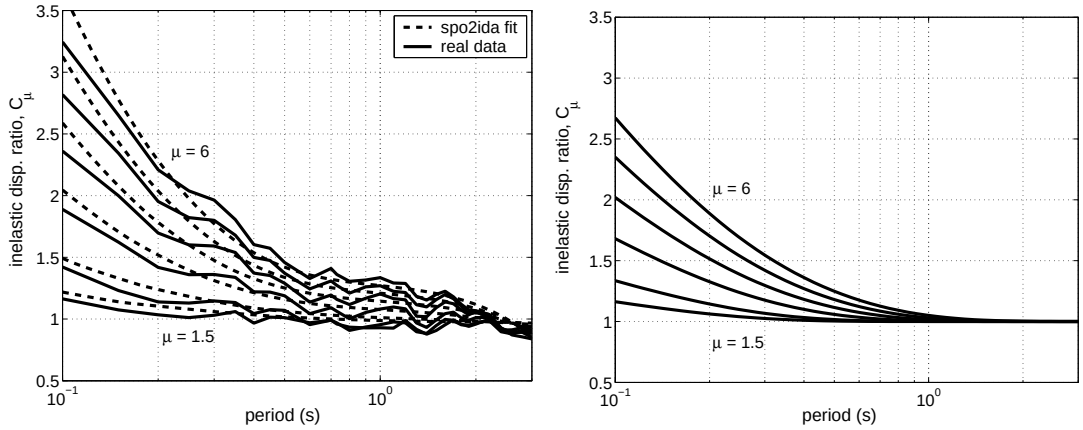

(a) Results from IDA versus SPO2IDA

(b) Results from Miranda [10]

Figure 6. Comparing estimates of mean C_μ ratios generated by SPO2IDA for the special elastic-perfectly-plastic case versus the real data and results from Miranda [10] for $\mu = 1.5, 2, 3, 4, 5, 6$.

In Figure 6(a) we have used Equation (12) to calculate average C_μ ratios using SPO2IDA for an elastic-perfectly-plastic system over a range of periods from 0.1s to 3s using SPO2IDA. On the same figure we also plot the average C_μ calculated directly from the 30 record suite through IDA, without the use of any approximation or fit. Clearly, the SPO2IDA results closely match the exact ones, except perhaps for the shortest of periods. As a further comparison, we have recreated in Figure 6(b) the C_μ results from the proposed equation in Miranda [10], generated for an elastic-perfectly-plastic model with kinematic hardening, using over 200 records that have a wide magnitude and source-to-site distance range, and that were all recorded on firm soil. As expected, the results are comparable

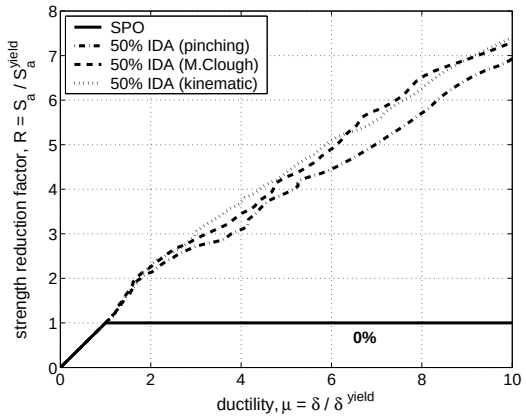

(a) Three hysteresis models for elastic-perfectly-plastic system, $a_h = 0$, $T = 1$s.

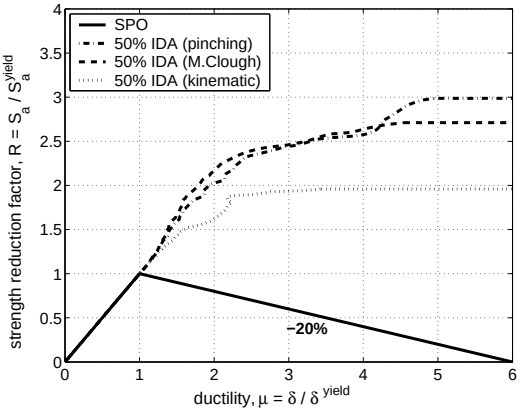

(b) Three hysteresis models for elastic-negative system, $a_c = -0.2$, $T = 1$s.

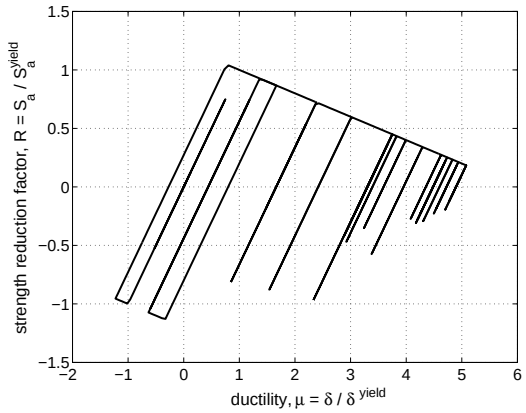

(c) Kinematic hysteresis for elastic-negative system, $a_c = -0.2$, $T = 1$s for record #29 at intensity $R = 2.4$.

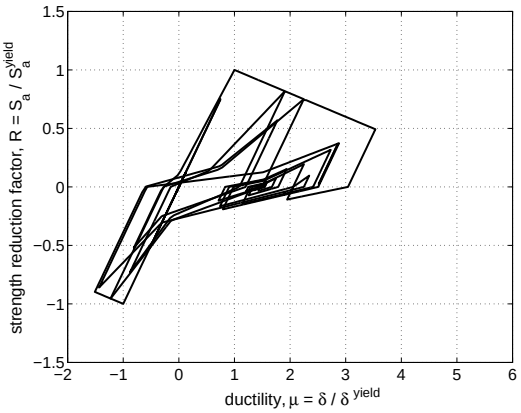

(d) Pinching hysteresis for elastic-negative system, $a_c = -0.2$, $T = 1$s for record #29 at intensity $R = 2.4$.

Figure 7. The different effect of the hysteresis model on oscillators with elastic-perfectly-plastic and elastic-negative backbones.

everywhere but in the short period range, where the record-to-record variability is maximum. Of course, such a specialized fit should be expected to outperform SPO2IDA, especially in the short periods. Still, our tool is proven to be suited to many applications, even beyond estimating the fractile IDAs that it was originally designed for.

6. LIMITS OF APPLICABILITY

By mostly focusing on the oscillator backbone we have restricted our effort in several other aspects; ground motion records were selected from a narrow magnitude and distance bin and correspond to firm

soil only, while hysteresis-wise, we have only considered a 5% damped, moderately pinching model. Some of these choices may have a significant impact on the response of oscillators thus accordingly restricting the applicability of SPO2IDA.

Regarding the selection of the records, the issue of magnitude, source-to-site distance and soil site appear. Only the case of the elastic-perfectly-plastic and the elastic-hardening system have been documented in the literature: The resulting mean R-factor, C_μ and C_R are not significantly influenced by magnitude, except maybe in the shorter periods (Ruiz-Garcia and Miranda [25]), or distance, unless near-fault directivity exists (e.g., Nassar and Krawinkler [4], Miranda [10]). Still, such issues remain open when dealing with the post-peak response. Regarding the soil-site, Miranda [10] has found little dependance within different firm soil sites, but Miranda [26] and Rahnama and Krawinkler [27] confirm that soft soil sites can be significantly different and their effect needs to be taken into account when applicable.

The oscillator hysteresis details, e.g., the degree (or existence) of pinching or the cyclic deterioration, are another interesting issue. For example, for a moderate period elastic-perfectly-plastic system (Figure 7(a)) the effect of using a pinching, a modified Clough or a kinematic model [27] is practically negligible; they generate the same median (and similarly all fractile) IDA curves. For an elastic-negative backbone, as shown in Figure 7(b), the median IDA (and actually any individual IDA curve) of the kinematic shows consistently higher μ-demands and lower R-capacities, while the other two models are quite similar. Figure 7(c) shows that on the descending branch of the backbone the kinematic model cannot maintain the full loops achieved by the pinching (Figure 7(d)) or the modified Clough models [see also 27–29], thus arriving to an early collapse. In general, various hysteretic details may become an important parameter once we go past the peak of the backbone, while others may remain insignificant. For a more comprehensive treatment of this issue the reader is referred to Ibarra [13].

7. CONCLUSIONS

A complete methodology has been presented that accurately accounts for the effect of the backbone on the seismic behavior of an oscillator with arbitrary period. The investigated backbone shapes range from simple bilinear to complex quadrilinear with an elastic, a hardening and a negative-stiffness segment plus a final residual plateau that terminates with a drop to zero strength. It was found that (1) long hardening segments significantly improve performance, while their slope has only a small effect, (2) the steeper the slope of the negative-stiffness segment, the higher the demands and the lower the capacities past the peak of the backbone, (3) residual plateaus that are higher in terms of strength or longer in terms of ductility, both benefit the post-peak performance and (4) the oscillator period significantly influences the effect of all segments except the hardening one in the moderate or long period ranges. Probably the most important fact is that (5) many different backbones exist that produce similar dynamic behavior, often defying current engineering intuition. Thus, only some basic backbone shapes need to be investigated, allowing a complete quadrilinear backbone to be captured with only a handful of equations. The result is a flexible, publicly available software tool for performing fast assessments of the (median and dispersion of) demand and capacity of virtually any oscillator. In conjunction with an appropriate methodology that extends predictions to MDOF structures (Vamvatsikos and Cornell [30]), an engineer-user is able to effortlessly get an accurate, spreadsheet-level estimate of seismic performance without having to perform the costly analyses, providing ready insights into the relative advantages and disadvantages of possible design or retrofit alternatives.

ACKNOWLEDGEMENTS

Financial support for this research was provided by the sponsors of the Reliability of Marine Structures Affiliates Program of Stanford University. We would also like to thank Doctor L. Ibarra and Professors H. Krawinkler, A. Ayoub for providing the SDOF analysis program.

REFERENCES

1. Vamvatsikos D, Cornell CA. Incremental dynamic analysis. *Earthquake Engineering and Structural Dynamics* 2002; **31**(3):491–514.
2. FEMA. NEHRP guidelines for the seismic rehabilitation of buildings. *Report No. FEMA-273*, Federal Emergency Management Agency, Washington DC, 1997.
3. Riddell R, Newmark NM. Statistical analysis of the response of nonlinear systems subjected to earthquakes. *Structural Research Series No. 468*, University of Illinois at Urbana-Champaign, Urbana, IL, 1979.
4. Nassar AA, Krawinkler H. Seismic demands for SDOF and MDOF systems. *Report No. 95*, The John A.Blume Earthquake Engineering Center, Stanford University, Stanford, CA, 1991.
5. Lee LH, Han SW, Oh YH. Determination of ductility factor considering different hysteretic models. *Earthquake Engineering and Structural Dynamics* 1999; **28**(9):957–977.
6. Al-Sulaimani GJ, Roessett JM. Design spectra for degrading systems. *ASCE Journal of Structural Engineering* 1985; **111**(12):2611–2622.
7. Miranda E, Akkar S. Dynamic instability of simple structural systems. *ASCE Journal of Structural Engineering* 2003; **129**(12):1722–1726.
8. Newmark NM, Hall WJ. *Earthquake Spectra and Design*. Earthquake Engineering Research Institute: Berkeley, CA, 1982.
9. Vidic T, Fajfar P, Fischinger M. Consistent inelastic design spectra: Strength and displacement. *Earthquake Engineering and Structural Dynamics* 1994; **23**(5):507–521.
10. Miranda E. Inelastic displacement ratios for structures on firm sites. *ASCE Journal of Structural Engineering* 2000; **126**(10):1150–1159.
11. Vamvatsikos D, Cornell CA. Applied incremental dynamic analysis. *Earthquake Spectra* 2004; **20**(2):523–553.
12. Veletsos AS, Newmark NM. Effect of inelastic behavior on the response of simple systems to earthquake motions. In *Proceedings of the 2nd World Conference on Earthquake Engineering*. Tokyo, Japan, 1960; 895–912.
13. Ibarra LF. Global collapse of frame structures under seismic excitations. PhD Dissertation, Department of Civil and Environmental Engineering, Stanford University, Stanford, CA, 2003.
14. Stear JD, Bea RG. A simplified structural analysis method for jacket–type platforms in seismically–active regions. *Report to Joint Industry Project sponsors*, Marine Technology and Management Group, Department of Civil and Environmental Engineering, University of California, Berkeley, CA, 1999.
15. Farin G. *Curves and Surfaces for Computer Aided Geometric Design: A Practical Guide* (2nd edn). Academic Press: San Diego, CA, 1990.
16. Vamvatsikos D. Seismic performance, capacity and reliability of structures as seen through incremental dynamic analysis. PhD Dissertation, Department of Civil and Environmental Engineering, Stanford University, Stanford, CA, 2002. http://www.stanford.edu/group/rms/Thesis/Dimitrios-1side.pdf or http://blume.stanford.edu/pdffiles/Tech%20Reports/TR151_Vamvatsikos.pdf [Jan 2006].
17. Vamvatsikos D. SPO2IDA software for moderate periods, 2001. http://blume.stanford.edu/pdffiles/Tech%20Reports/TR151_spo2ida-mt.xls [Jan 2006].
18. Vamvatsikos D. SPO2IDA software for moderate periods, online version, 2001. URL http://tremble.stanford.edu/cgi-bin/spo2ida-mt.pl. [Jan 2006].
19. Efron B, Tibshirani RJ. *An Introduction to the Bootstrap*. Chapman & Hall/CRC: New York, 1993.
20. Weisberg S. *Applied Linear Regression* (2nd edn). John Wiley & Sons: New York, 1985.
21. Vamvatsikos D. SPO2IDA software for short, moderate and long periods, 2002. http://blume.stanford.edu/pdffiles/Tech%20Reports/TR151_spo2ida-allt.xls [Jan 2006].
22. Miranda E. Estimation of inelastic deformation demands of SDOF systems. *ASCE Journal of Structural Engineering* 2001; **127**(9):1005–1012.
23. Shome N, Cornell CA. Probabilistic seismic demand analysis of nonlinear structures. *Report No. RMS-35*, RMS Program, Stanford University, Stanford, CA, 1999. http://www.stanford.edu/group/rms/Thesis/NileshShome.pdf [Jan 2006].
24. Benjamin JR, Cornell CA. *Probability, Statistics, and Decision for Civil Engineers*. McGraw-Hill: New York, 1970.
25. Ruiz-Garcia J, Miranda E. Inelastic displacement ratios for evaluation of existing structures. *Earthquake Engineering and Structural Dynamics* 2003; **32**(8):1237–1258.

26. Miranda E. Evaluation of site-dependent inelastic seismic design spectra. *ASCE Journal of Structural Engineering* 1993; **119**(5):1319–1338.
27. Rahnama M, Krawinkler H. Effects of soft soils and hysteresis model on seismic demands. *Report No. 108*, The John A.Blume Earthquake Engineering Center, Stanford University, Stanford, CA, 1993.
28. Mahin SA, Lin J. Construction of inelastic response spectra for single-degree-of-freedom systems: computer program and applications. *Report UCB/EERC-83/17*, Earthquake Engineering Research Center, University of California, Berkeley, CA, 1983.
29. Krawinkler H, Seneviratna GDPK. Pros and cons of a pushover analysis of seismic performance evalation. *Engineering Structures* 1998; **20**(4-6):452–464.
30. Vamvatsikos D, Cornell CA. Direct estimation of the seismic demand and capacity of MDOF systems through incremental dynamic analysis of an SDOF approximation. *ASCE Journal of Structural Engineering* 2005; **131**(4):589–599.

